Parasuraman, B, Pazhani, A, Michael, AX, Pitchaimuthu, S and Batako, A

Effect of T6 and T8 Ageing on the Mechanical and Microstructural Properties of Graphene-Reinforced AA2219 Composites for Hydrogen Storage Tank Inner Liner Applications

Journal of
Composites Science

MDPI

Article

Effect of T6 and T8 Ageing on the Mechanical and Microstructural Properties of Graphene-Reinforced AA2219 Composites for Hydrogen Storage Tank Inner Liner Applications

Bharathiraja Parasuraman [1], Ashwath Pazhani [2,*], Anthony Xavior Michael [1,*], Sudhagar Pitchaimuthu [3] and Andre Batako [4]

[1] School of Mechanical Engineering, Vellore Institute of Technology, Vellore TN-632014, India; bharathiraja.p@vit.ac.in
[2] Faculty of Engineering, Environment and Computing, Coventry University, Coventry CV1 5FB, UK
[3] School of Engineering & Physical Sciences, Institute of Mechanical, Process & Energy Engineering, Heriot-Watt University, Riccarton EH14 4AS, UK
[4] General Engineering Research Institute, Liverpool John Moores University (LJMU), Liverpool L3 5UX, UK; a.d.batako@ljmu.ac.uk
* Correspondence: ae0255@coventry.ac.uk (A.P.); manthonyxavior@vit.ac.in (A.X.M.)

Abstract

This study examines the mechanical and microstructural properties of graphene-reinforced AA2219 composites developed for hydrogen storage tank inner liner applications. A novel processing route combining high-energy ball milling, ultrasonic-assisted stir casting, and squeeze casting was used to achieve homogeneous dispersion of 0.5 wt.% graphene nanoplatelets and minimise agglomeration. The composites were subjected to T6 and T8 ageing treatments to optimize their properties. Microstructural analysis revealed refined grains, uniform Al_2Cu precipitate distribution, and stable graphene retention. Mechanical testing showed that the as-cast composite exhibited a UTS of 308.6 MPa with 13.68% elongation. After T6 treatment, the UTS increased to 353.6 MPa with an elongation of 11.24%. T8 treatment further improved the UTS to 371.5 MPa, with an elongation of 8.54%. Hardness improved by 46%, from 89.6 HV (as-cast) to 131.3 HV (T8). Fractography analysis indicated a shift from brittle to ductile fracture modes after heat treatment. The purpose of this work is to develop lightweight, high-strength composites for hydrogen storage applications. The novelty of this study lies in the integrated processing approach, which ensures uniform graphene dispersion and superior mechanical performance. The results demonstrate the suitability of these composites for advanced aerospace propulsion systems.

Keywords: aluminium 2219 alloy; graphene; stir-squeeze casting; T6 and T8 ageing; ball milling; hardness and UTS; microstructure analysis

Academic Editor: Jinyang Xu

Received: 1 June 2025
Revised: 23 June 2025
Accepted: 24 June 2025
Published: 25 June 2025

Citation: Parasuraman, B.; Pazhani, A.; Michael, A.X.; Pitchaimuthu, S.; Batako, A. Effect of T6 and T8 Ageing on the Mechanical and Microstructural Properties of Graphene-Reinforced AA2219 Composites for Hydrogen Storage Tank Inner Liner Applications. *J. Compos. Sci.* **2025**, *9*, 328. https://doi.org/10.3390/jcs9070328

1. Introduction

Aluminium and its alloys are vital in modern industry due to their low density, high strength-to-weight ratio, and corrosion resistance. In aerospace, they are crucial for airframes and rocket structures, enabling significant weight savings. The automotive sector uses them in engine blocks, pistons, and chassis for better fuel efficiency. Military and defence industries benefit from their strength in armoured vehicles and protective components. Aluminium-based composites enhance wear resistance in engine parts like pistons and brake drums. Additionally, their use in electronics for heat sinks, as well as in energy

storage, marine, and infrastructure applications, highlights their versatility and growing technological importance [1–3]. Aluminium alloy 2219 (AA2219) is a high-strength aluminium–copper alloy containing 5.8–6.8 wt.% Cu with trace Ti, V, and Zr additions and is renowned for its high specific strength, excellent weldability, and fracture toughness from cryogenic to elevated temperatures, making it a material of choice in aerospace and automotive applications [4,5]. The base alloy demonstrates excellent mechanical characteristics, including good weldability, high fracture toughness, and resistance to stress corrosion cracking, particularly in the T8 temper condition. With a density of 2.84 g/cm^3, 2219 aluminium offers a favourable strength-to-weight ratio that makes it particularly suitable for weight-critical applications [6]. The alloy maintains consistent performance across an impressive temperature range from cryogenic (−452 °F/−269 °C) to elevated temperatures (600 °F/316 °C), explaining its extensive use in aerospace components, including the Space Shuttle External Tank and various modules on the International Space Station [7,8]. To further enhance its performance, graphene nanoplatelets (Gr) have emerged as attractive nanoscale reinforcements owing to their exceptional Young's modulus (~1 TPa), tensile strength (~125 GPa), and thermal conductivity (~5000 $W \cdot m^{-1} \cdot K^{-1}$). In AA2219, ceramic reinforcements (Al_2O_3, TiC, SiC, ZrO_2) introduced via stir casting boost tensile strength by up to ~40% and hardness by 34–44%, though excessive loading can induce porosity and reduce ductility [9,10]. Graphene nanoplatelets (Grnp, ~0.5 wt.%) promise even greater gains but demand meticulous dispersion to prevent agglomeration-driven defects. During solution treatment (≈530 °C) and ageing, AA2219 follows the supersaturated-solution → G.P. zones → θ'' → θ' → θ sequence, with reinforcements acting as heterogeneous nucleation sites and thermal-mismatch dislocations that locally modify precipitation kinetics. When paired with T6/T8 ageing, optimal reinforcement fractions deliver peak hardness and tensile-strength improvements; beyond ~0.5 wt.% Grnp, agglomeration and porosity negate these benefits [11,12].

However, conventional stir-casting and powder-consolidation approaches often suffer from graphene agglomeration and poor matrix bonding, limiting the mechanical gains. Ultrasonic melt processing has demonstrated grain refinement and melt homogenization in large Al ingots, leveraging cavitation-enhanced nucleation, fragmentation and streaming effects. Nevertheless, most studies focus on direct-chill casting without post-casting pressure treatment, and scalable routes to uniform graphene dispersion in AA2219 remain underexplored. Squeeze casting under high pressure has shown up to 68% porosity reduction in Al–Li composites, yielding fine dendritic structures and near-defect-free castings [13–15]. Combining this with ultrasonic stirring could further improve graphene distribution, as hinted by reduced microporosity in hybrid MMCs. Meanwhile, powder-based methods such as ball milling plus spark plasma sintering produce near-theoretical densities but lack scalability and detailed crystallographic insight. Moreover, T6 (solution treatment + ageing) and T8 (pre-strain + ageing) protocols are known to control θ'-Al_2Cu precipitation in AA2219 [15–18].

Based on the literature, the intrinsically poor wettability of two-dimensional graphene nanoplatelets in molten aluminium often leads to agglomeration and non-uniform dispersion within the AA2219 matrix. Also, the density of graphene is lower compared to that of aluminium 2219 alloy. Due to this, graphene will float on the molten aluminium, which leads to the non-uniform dispersion of graphene in the matrix. To overcome this, we introduce a hybrid solid–liquid metallurgy route in which graphene is first ball milled onto AA2219 powder surfaces via high-energy planetary ball milling (HEPBM). Extended HEPBM not only reduces stacked graphene layers but also firmly anchors nanoplatelets onto aluminium particles, greatly improving their wetting behaviour [19]. The milled powder is then consolidated through ultrasonic-assisted stir casting, where cavitation

breaks up residual clusters, and squeeze casting, which collapses porosity and enhances interfacial bonding. This integrated approach yields AA2219–graphene composites with truly homogeneous graphene dispersion, providing a scalable raw-material ingot suitable for large-scale structural applications in the aerospace and automotive sectors, including launch-vehicle components; tailored T6 and T8 ageing was also used to improve the properties of the composites. In this research work, 0.5 wt.% of graphene reinforced with aluminium 2219 alloy composite was fabricated via ultrasonic-assisted stir and squeeze casting and then subjected to mechanical and microstructural property evaluation. The findings of this study are highly significant for industrial applications, as the developed graphene-reinforced AA2219 composites combine lightweight characteristics with enhanced strength and ductility. By utilizing scalable solid–liquid processing methods and optimized heat treatments, this work demonstrates a practical pathway to producing advanced materials suitable for hydrogen storage tank liners in aerospace propulsion. Moreover, the integrated approach can be adapted for mass production, offering valuable solutions for the automotive, defence, and energy sectors, where the demand for high-performance, lightweight materials is continuously increasing.

2. Materials and Methods

2.1. Materials Used

In this research work, to fabricate aluminium matrix composites (AMCs), the aluminium 2219 alloy is chosen as the matrix material and graphene nanoplatelets as reinforcement. The aluminium 2219 alloy ingot was procured from MatRICS, Tamil Nadu, India. It has a density of 2.84 g/cm^3. The 2D graphene nanoplatelets were procured from Angstron Materials Inc., Dayton, OH, USA. The average size of the graphene is 10 µm × 5 nm. The density of graphene is 2.26 g/cm^3. To prepare the powder mixture, aluminium 2219 alloy powder was procured from Ampal Inc., Palmerton, PA, USA. The shape of the powder particle is spherical, and the average size is 40–50 µm. In this study, 0.5 wt.% of graphene is reinforced with aluminium 2219 alloy powder, then this powder mixture is reinforced in the molten aluminium in the casting process. Figure 1 depicts the micrographs of the AA2219 alloy raw powder and graphene nanoplatelets [20]. The chemical composition the AA2219 alloys is presented in Table 1.

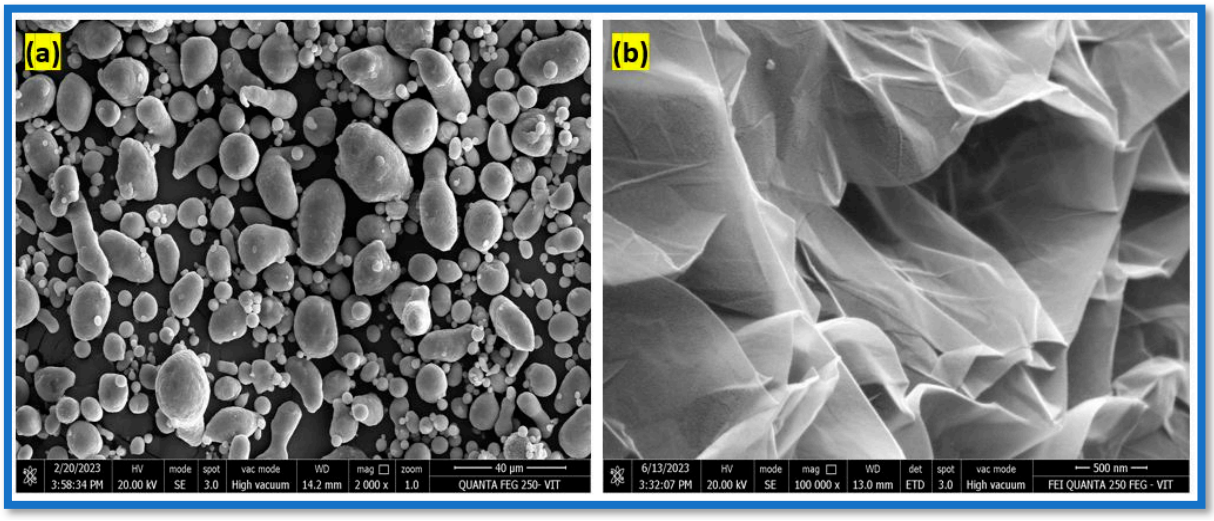

Figure 1. FE-SEM micrographs of (**a**) aluminium 2219 alloy powder and (**b**) graphene nanoplates.

Table 1. Chemical composition of AA2219 aluminium alloy (wt.%).

Cu	Si	Fe	Mg	Mn	Ti	Zn	Al
5.98	0.13	0.24	0.01	0.32	0.05	0.05	Bal

2.2. Methodology

Figure 2 shows the fabrication of the graphene-reinforced aluminium 2219 alloy matrix composite. The AA2219 alloy powder and graphene nanoplatelets were first precisely weighed to yield a 0.5 wt.% composite and lightly tumbled to break up large agglomerates. This blend was then fed into a high-speed homogenizer and mixed at 100 RPM for 60 min, promoting initial dispersion of the graphene platelets over the aluminium surfaces. The partially blended powder was transferred to a planetary ball mill with a 10:1 ball-to-powder ratio and milled at 250 RPM for a total of 2 h, divided into four 30 min runs interspersed with brief pauses to dissipate heat and prevent cold welding. Under an argon flow of 6 L/min, the furnace components were preheated: the furnace to 800 °C, the melt furnace to 750 °C, the reinforcement powder mixture to 250 °C, the preheat temperature of the mould is 300 °C, and that of the runner is 400 °C to minimise oxidation and thermal shock.

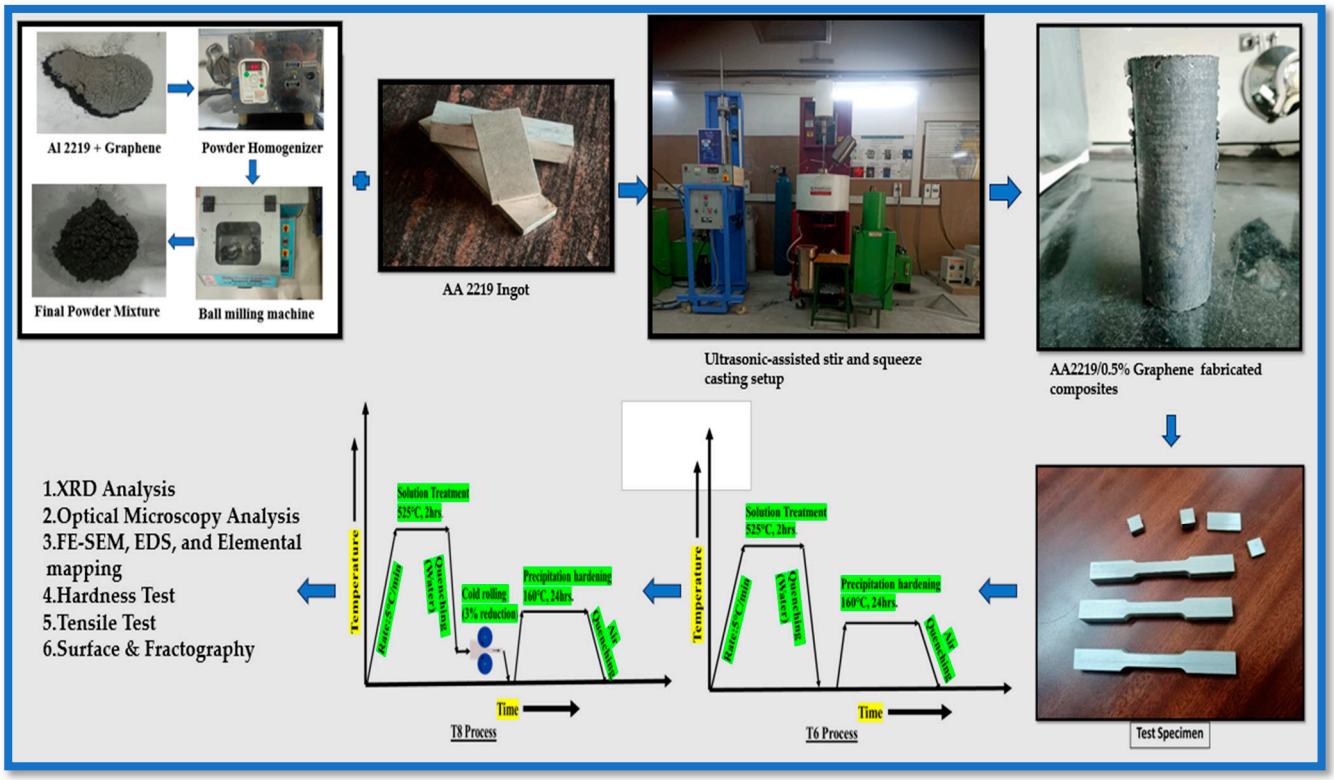

Figure 2. Schematic methodology of the fabrication of graphene-reinforced aluminium 2219 alloy matrix composites.

The preheated powder mixture was injected slowly into the 750 °C AA2219 melt while stirring with a graphite-coated SS 310 two-fin blade at 450 RPM for 10 min; the blade's vertical oscillation created a turbulent three-dimensional flow, suspending the powder and wetting each particle. Immediately thereafter, a 20 kHz, 2300 W ultrasonic probe was immersed in the melt for 180 s, where cavitation collapsed graphene agglomerates and expelled dissolved gases [15,18]. Finally, the homogenized melt was poured into the 300 °C preheated squeeze cast mould under continuous argon protection, and squeeze pressure was applied on the poured molten metal at 400 MPa, allowing it to solidify, yielding a

defect-free AA2219–graphene composite ingot with uniformly dispersed reinforcement and strong interfacial bonding. After solidification, the composite ingots were allowed to cool to room temperature under a continuous argon atmosphere to prevent oxidation. Once cooled, the ingots were removed from the mould and the specimens were sectioned, machined, and polished according to standard metallographic procedures to prepare them for subsequent microstructural characterization and mechanical testing [21–23].

2.3. Heat Treatment

Figure 3 depicts the heat treatment strategy for graphene-reinforced AA2219 matrix composites that was designed to optimize the microstructure and mechanical properties through tailored precipitation and work-hardening mechanisms. The T6 condition involved solution treatment at 525 °C for 2 h, followed by rapid water quenching to retain alloying elements in solid solution. Subsequent artificial ageing at 160 °C for 24 h facilitated controlled precipitation of strengthening phases such as Al_2Cu, enhancing hardness and strength. For the T8 condition, the process was modified by introducing a cold rolling step (3% reduction) after solution treatment and quenching.

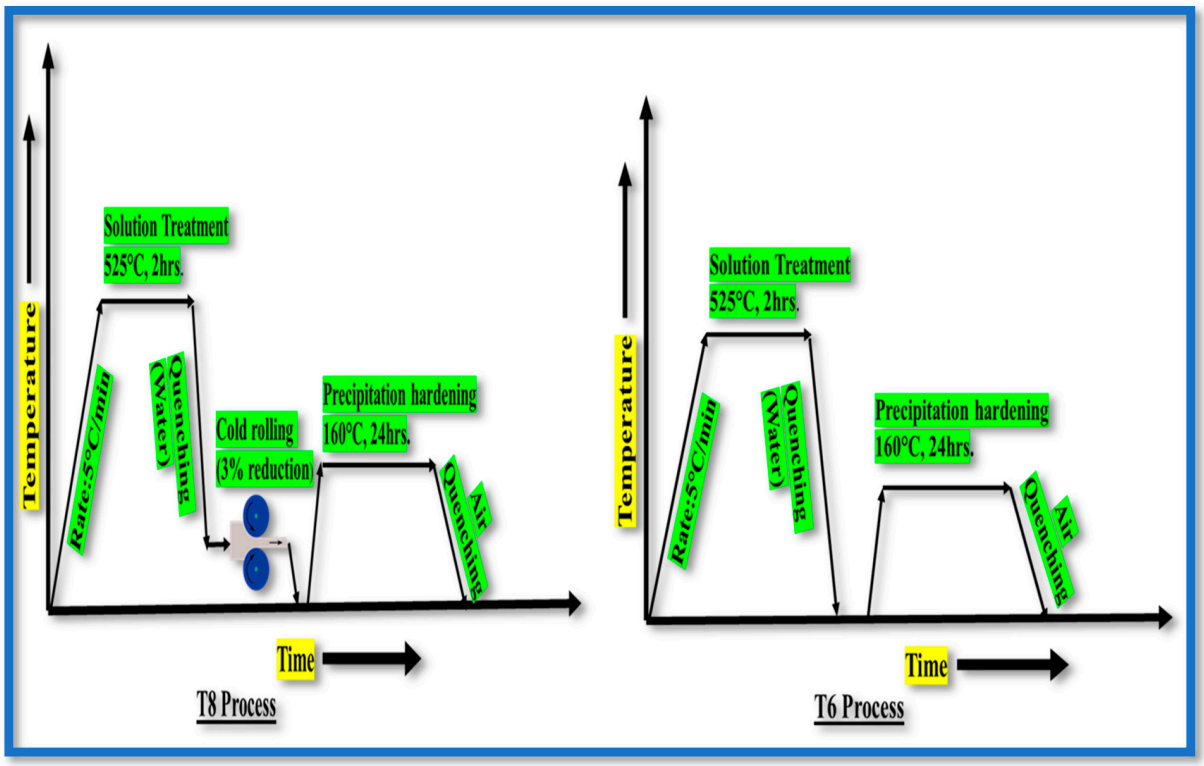

Figure 3. Heat-treatment process of AA2219/graphene matrix composites.

This additional deformation increased the dislocation density and provided extra nucleation sites for precipitate formation during ageing. Artificial ageing at 160 °C for 24 h was then carried out, followed by air quenching. The combined effect of cold rolling and precipitation hardening in T8 resulted in a finer and more uniform dispersion of precipitates compared to T6. These heat treatment regimes were carefully selected to maximise the synergistic strengthening from both graphene reinforcement and optimized precipitate distribution. This dual approach not only enhances the load transfer efficiency at the graphene–matrix interface but also inhibits grain growth, leading to superior mechanical performance [24].

3. Results and Discussion

3.1. XRD Analysis

The X-ray diffraction machine was operated from 10° to 90° at 30 mA and 40 kV with a scan speed of 2°/min to identify the phases and crystallographic changes in both the as-cast and the heat-treated composites. The X-ray diffraction (XRD) analysis of the AA2219 aluminium alloy reinforced with 0.5 wt.% graphene, as shown in Figure 4, confirms the presence of three primary phases—aluminium (Al), graphene, and Al_2Cu—across the as-cast and T6 and T8 heat-treated conditions. The aluminium matrix (JCPDS 04-0787) exhibits prominent peaks at 2θ values of approximately 38.4° (111), 44.7° (200), 65.1° (220), and 78.2° (311), while the graphene phase (JCPDS 75-1621) is identified by its (002) plane at around 26.5° of 2θ. The Al_2Cu intermetallic phase (JCPDS 25-0012) is observed at 2θ positions near 41.5° (110) and 47.5° (211). In the as-cast condition, the XRD peaks are broader and less intense, reflecting finer crystallite size and higher micro-strain due to rapid solidification and lattice defects [25].

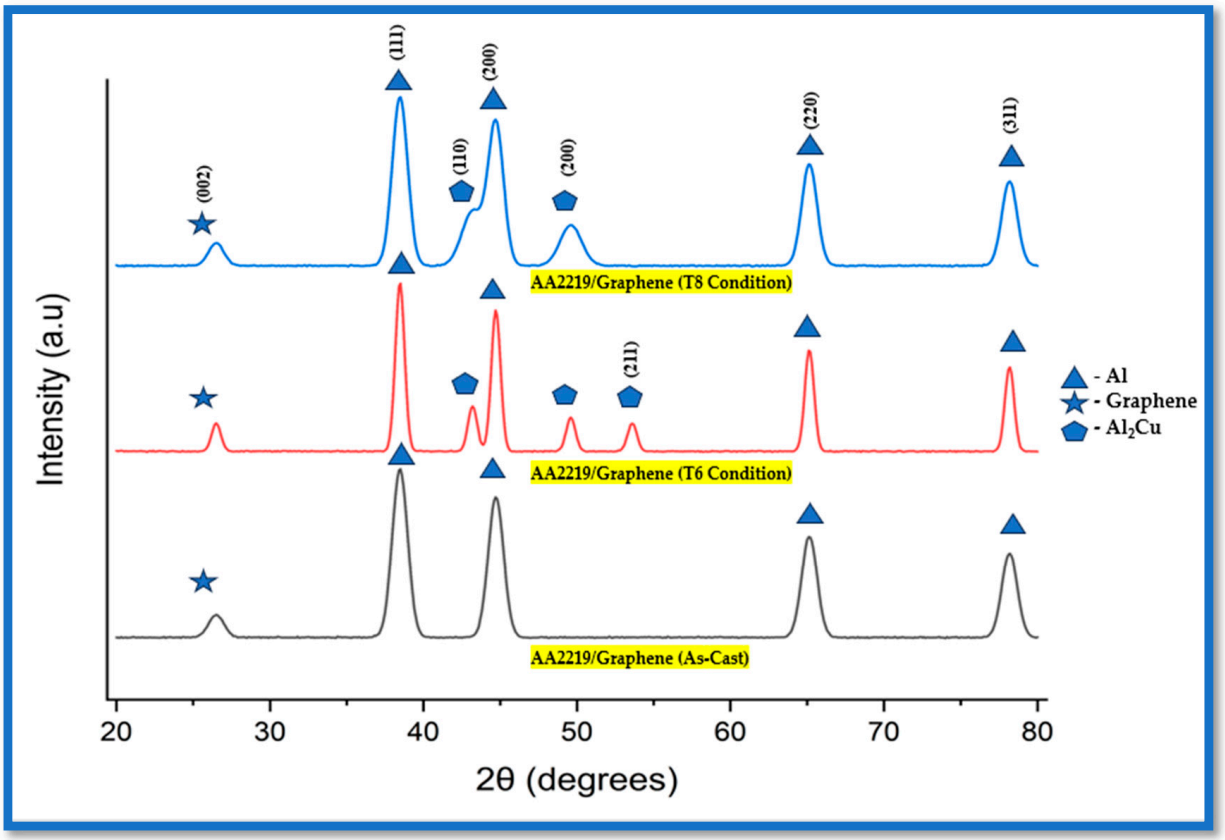

Figure 4. XRD analysis of AA2219/graphene matrix composites.

This broadening is attributed to both small crystallite domains, as described by the Scherrer equation, and localized lattice distortions. With T6 and T8 heat treatments, the aluminium peaks become sharper and more intense, indicating grain growth, reduction in micro-strain, and improved crystallinity as atomic rearrangement and defect reduction occur during solution treatment, cold working, and ageing. Notably, after the T8 condition, the peaks corresponding to the Al_2Cu precipitates become broader compared to T6, which indicates the formation of coarser Al_2Cu particles within the matrix. This peak broadening for Al_2Cu after T8 reflects the over-ageing or coarsening of precipitates due to the combined effects of deformation and ageing. The consistent presence of the graphene (002) peak across all conditions demonstrates effective retention and stability of graphene throughout

processing [26]. Additionally, the absence of peaks corresponding to undesirable phases such as harmful aluminium carbides or oxides indicates good phase stability and minimal interfacial reactions.

3.2. Optical Microscopy Analysis

The as-cast and heat-treated specimens were prepared for microstructural examination by sequentially polishing them with abrasive papers ranging from 200 to 2000 grit, followed by final smoothing on a disc polishing machine. After polishing, the samples were etched with Keller's reagent to reveal their macrostructure, and the resulting microstructures were observed using an Olympus BX53M optical microscope. Figure 5 presents optical micrographs highlighting the progressive grain refinement and structural evolution in the AA2219–0.5 wt.% graphene composite under different heat-treatment conditions. The as-cast microstructure (Figure 5a) comprises relatively coarse, equiaxed grains averaging ~75 μm in size, with evident heterogeneity and dendritic remnants, contributing modestly to strength through limited grain-boundary impediment of dislocation motion. Subsequent T6 heat treatment (Figure 5b) significantly refines the grain structure (~50 μm average grain size), owing to recrystallization during solution treatment, leading to improved homogeneity and enhanced Hall–Petch strengthening.

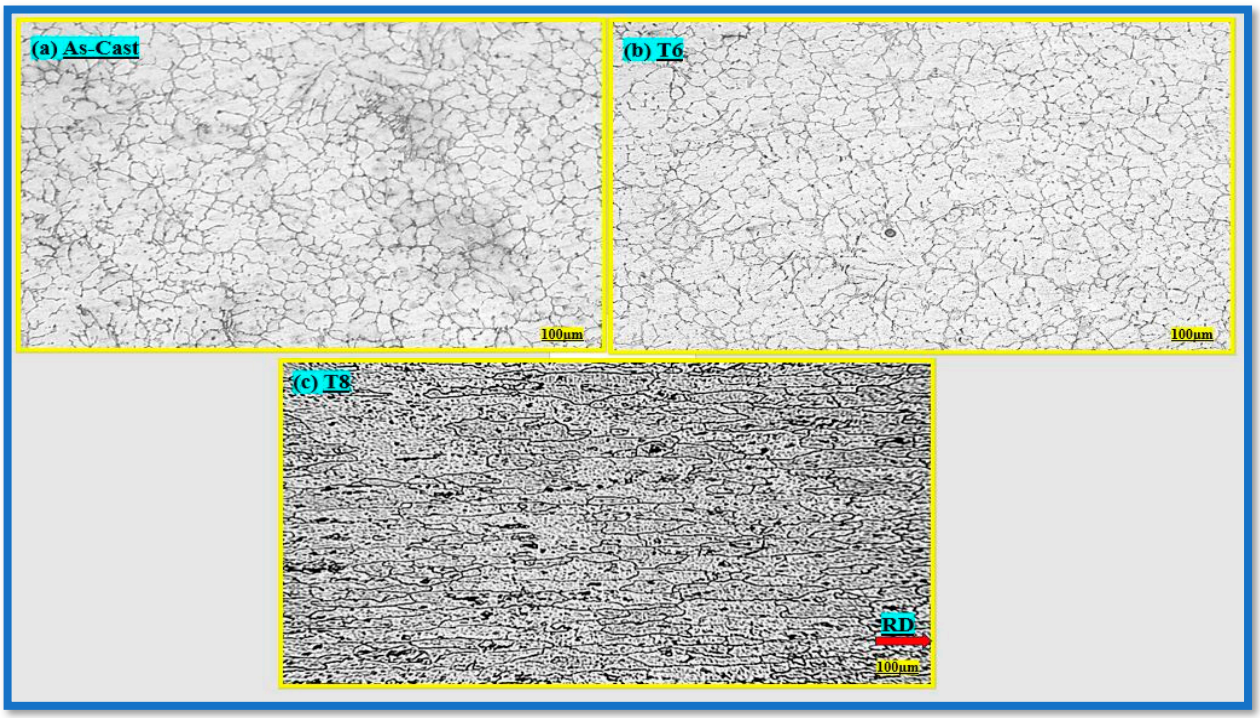

Figure 5. Optical macrographs of AA2219/graphene composites: (**a**) as-cast, (**b**) T6, and (**c**) T8.

In the T8 condition (Figure 5c), the introduction of prior cold working followed by ageing generates highly elongated, fibre-like subgrain structures (~21 μm average width), densely populated with dislocation walls and θ′ precipitates aligned along the rolling direction. This refined, banded subgrain morphology elevates strength via pronounced back-stress and forest-hardening effects. Additionally, dynamic strain ageing (DSA), manifested as Portevin–Le Chatelier (PLC) serrations, contributes to the composite's improved work-hardening characteristics, while residual stresses due to thermal mismatch between graphene and aluminium further impede dislocation glide [27,28]. Collectively, these microstructural mechanisms and stress interactions synergistically enhance the mechanical properties of the graphene-reinforced AA2219 alloy composites.

3.3. FE-SEM Analysis

The evolution of microstructure in AA2219 alloy under different processing conditions is distinctly evident in the SEM images. In the as-cast condition (Figure 6a), the microstructure is characterized by coarse, irregular grains interspersed with regions of clustered particles, indicative of inhomogeneous solidification and a limited grain-boundary area. This structure often translates into suboptimal mechanical properties, as dislocation movement is less effectively hindered by the sparse grain boundaries and particle agglomerates. Upon subjecting the alloy to T6 heat treatment (Figure 6b), a remarkable transformation occurs: the grains become significantly finer and more equiaxed, while the overall structure appears much cleaner and more uniform. This grain refinement can be attributed to the dissolution of coarse secondary phases during solutionising and the subsequent precipitation of fine, uniformly distributed strengthening particles during ageing. Such changes are critical, as they enhance both strength and toughness by increasing the number of barriers to dislocation motion. Further processing through the T8 route (Figure 6c), which couples cold working with artificial ageing, results in a pronounced elongation of the grains along the rolling direction and a further refinement of grain boundaries. This combination of work-hardening and precipitation not only raises the dislocation density but also locks the dislocations in place through the formation of finely dispersed precipitates. As a result, the T8-treated alloy exhibits the most refined and directionally aligned grain structure, which is directly linked to superior mechanical performance [29].

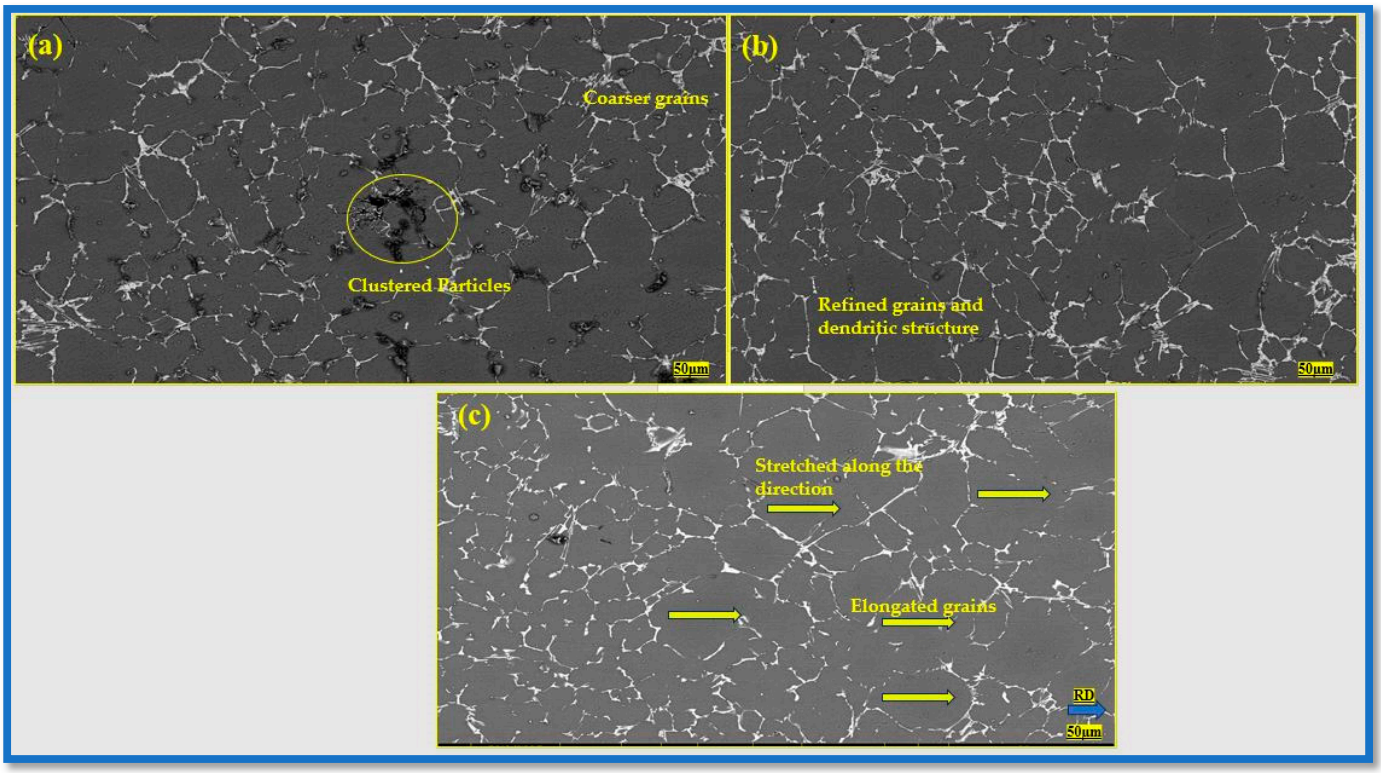

Figure 6. FE-SEM micrographs of AA2219/graphene composites: (**a**) as-cast, (**b**) T6, and (**c**) T8.

Overall, the progression from as-cast to T6 and T8 conditions clearly demonstrates how carefully designed heat treatment and mechanical processing routes can tailor the grain structure and, consequently, optimize the properties of AA2219 alloys for advanced engineering applications.

Figure 7 depicts the EDS elemental mapping of the graphene-reinforced AA2219 alloy, confirming the uniform distribution of major elements—Al, Cu, Mg and Si—across the

matrix, with clear evidence of carbon incorporation from the graphene reinforcement. Oxygen is observed in minor amounts, likely associated with surface oxides or processing residues. The strong, continuous presence of aluminium highlights the alloy's matrix integrity, while the discrete and homogeneously dispersed carbon signals reflect effective graphene dispersion without significant agglomeration. Trace elements such as Cu, Mg, and Si are also evenly distributed, supporting the homogeneity of the composite. The corresponding EDS spectrum quantitatively validates the composition, with aluminium as the dominant element, and confirms the successful retention of reinforcement and alloying constituents.

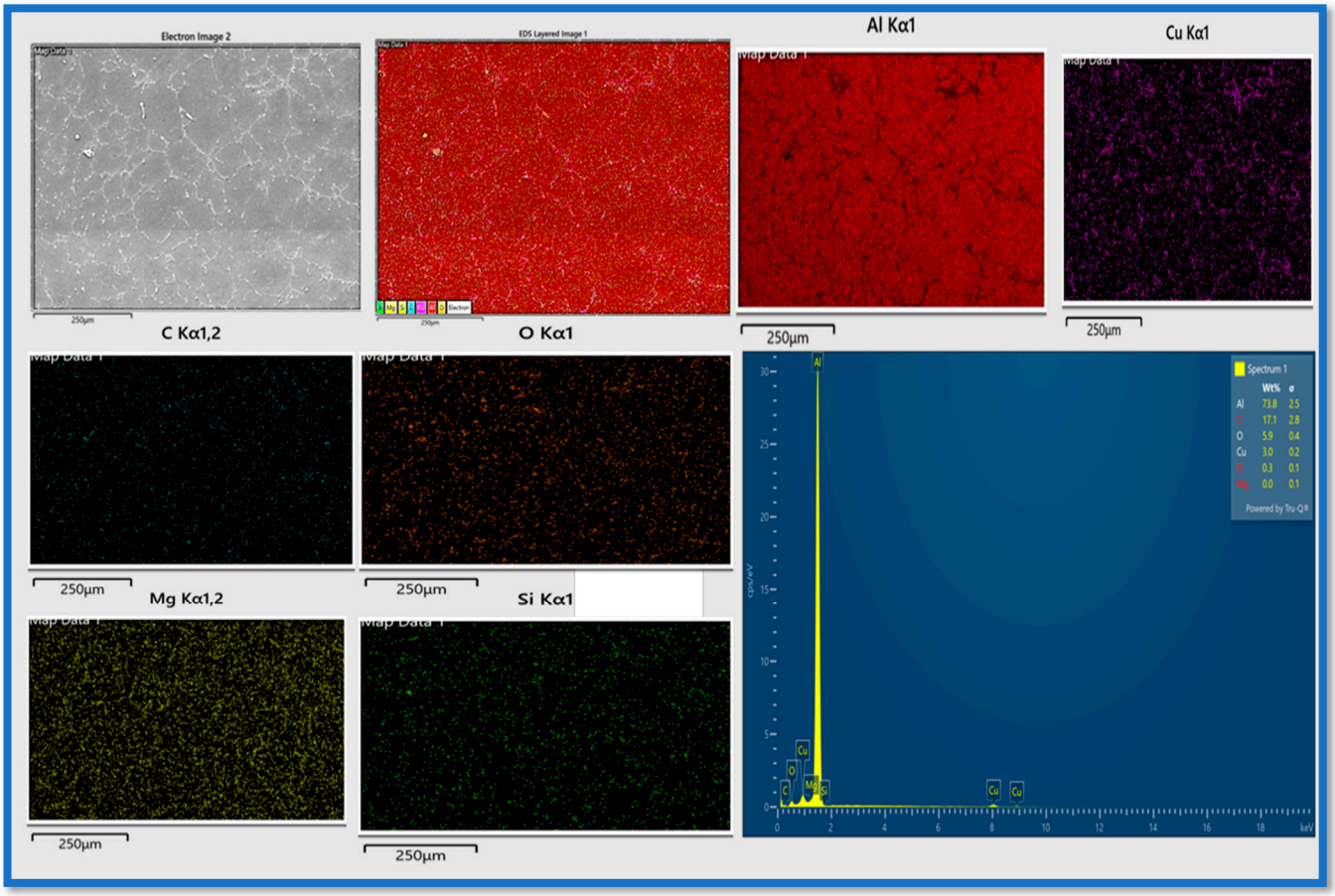

Figure 7. EDS analysis with elemental mapping of AA2219/graphene matrix composites.

Figure 8 presents the Point EDS analysis performed on the AA2219–graphene composite after T8 heat treatment and reveals significant compositional variations, confirming the presence of Al_2Cu precipitates at multiple sites. The high copper content observed in Spectrums 2 and 3 (36.48 wt.% and 51.10 wt.%, respectively) alongside substantial aluminium confirms the localized enrichment characteristic of Al_2Cu phases. Oxygen is also detected, likely due to minor surface oxidation or sample preparation effects. For the T8 sample, quantitative image analysis revealed a grain-boundary area fraction of 84.2% and a fine microstructure area fraction of 23.4%. These results confirm the effectiveness of the applied processing route in producing a highly refined and elongated grain structure with significant areas of fine microstructure. These results demonstrate the effective precipitation and distribution of strengthening phases, which are crucial for enhanced mechanical performance in the T8 condition. The combined EDS data validates that the microstructural refinement achieved during heat treatment leads to the formation of key intermetallics that underpin the composite's improved properties.

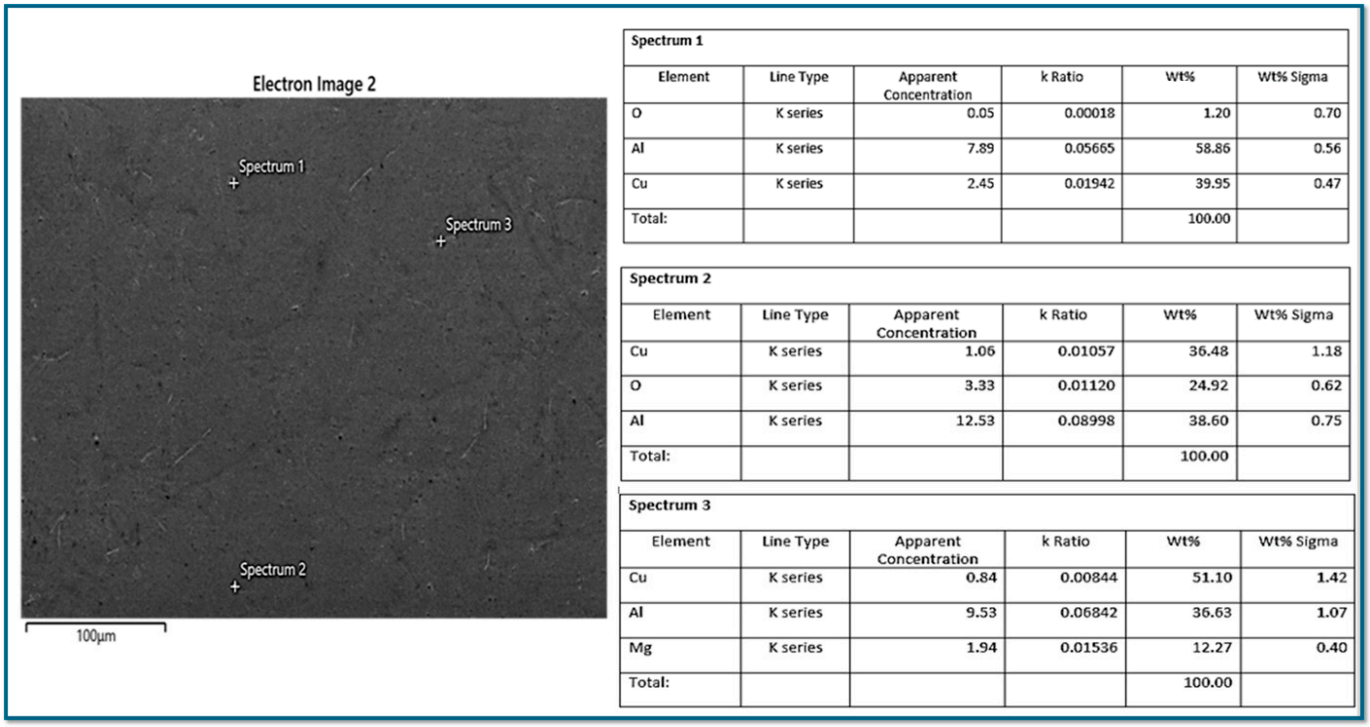

Spectrum 1

Element	Line Type	Apparent Concentration	k Ratio	Wt%	Wt% Sigma
O	K series	0.05	0.00018	1.20	0.70
Al	K series	7.89	0.05665	58.86	0.56
Cu	K series	2.45	0.01942	39.95	0.47
Total:				100.00	

Spectrum 2

Element	Line Type	Apparent Concentration	k Ratio	Wt%	Wt% Sigma
Cu	K series	1.06	0.01057	36.48	1.18
O	K series	3.33	0.01120	24.92	0.62
Al	K series	12.53	0.08998	38.60	0.75
Total:				100.00	

Spectrum 3

Element	Line Type	Apparent Concentration	k Ratio	Wt%	Wt% Sigma
Cu	K series	0.84	0.00844	51.10	1.42
Al	K series	9.53	0.06842	36.63	1.07
Mg	K series	1.94	0.01536	12.27	0.40
Total:				100.00	

Figure 8. Point EDS analysis of AA2219/graphene-T8 matrix composites.

In Figures 7 and 8, the characterization of the surfaces and interfaces between aluminium and graphene in the composite is shown, which was carried out using a combination of high-resolution microscopy and elemental analysis techniques. Field Emission Scanning Electron Microscopy (FE-SEM) and Energy Dispersive Spectroscopy (EDS) elemental mapping were utilized to examine the dispersion of graphene nanoplatelets and directly observe the interfacial regions. In the microstructural analysis, the presence of distinct, continuous carbon-rich layers at the grain boundaries and within the aluminium matrix confirms the successful integration and distribution of graphene. EDS mapping further supports this observation by showing localized enrichment of carbon at these interfaces, indicating the retention and stability of graphene after processing. Additionally, the absence of unwanted interfacial reaction products (such as aluminium carbide or oxide phases) was confirmed by X-ray diffraction (XRD), supporting the chemical stability of the interface. The effectiveness of the interface is also indirectly evidenced by mechanical testing results and fractography. Improved load transfer, as reflected in the enhanced tensile strength and ductility, suggests strong interfacial bonding. Post-fracture FE-SEM images reveal crack deflection and bridging phenomena at the graphene–aluminium interface, which further demonstrates good adhesion and effective stress distribution across the interface. Together, these microstructural, compositional, and mechanical observations provide comprehensive evidence for the formation of well-bonded and stable interfaces between aluminium and graphene in the composite.

3.4. Hardness Analysis

Vickers microhardness testing was performed on the as-cast and T6 and T8 heat-treated matrix composites using a Mitutoyo HB-210 microhardness tester and The equipment was sourced from Mitutoyo South Asia Pvt. Ltd., Chennai, India. For each sample, ten indentations were made under a 200 gf load with a diamond indenter, holding the load for 15 s before measurement. The Vickers microhardness results for the AA2219 alloy reinforced with 0.5 wt.% graphene, as shown in Figure 9 and Table 2, highlight the significant effect of heat treatment on the composite's hardness. The composite, fabricated by ultrasonic-

assisted stir and squeeze casting using a ball-milled graphene-AA2219 powder mixture to ensure uniform reinforcement distribution and prevent graphene flotation, exhibited a marked increase in hardness with post-casting heat treatment. The as-cast sample had a microhardness of 89.6 HV. After T6 heat treatment, the hardness increased to 114.2 HV, and further enhancement was observed in the T8 condition, the microhardness reaching 131.3 HV. This is a progressive improvement of over 46% from the as-cast to the T8 specimens. This systematic improvement can be attributed to multiple synergistic strengthening mechanisms operating simultaneously in the graphene-reinforced AA2219 composite. The ball-milling process for mechanical alloying ensures uniform dispersion of graphene nanoplatelets within the aluminium matrix while preventing agglomeration and flotation issues during casting, thereby establishing an effective load transfer interface between the high-strength graphene reinforcement and the aluminium matrix. The ultrasonic-assisted stir casting further enhances the wetting characteristics and interfacial bonding, enabling efficient stress transfer from the soft aluminium matrix to the rigid graphene platelets through shear lag mechanisms. Additionally, the graphene nanoplatelets act as heterogeneous nucleation sites, promoting grain refinement and increasing the grain boundary density, which contributes to Hall–Petch strengthening.

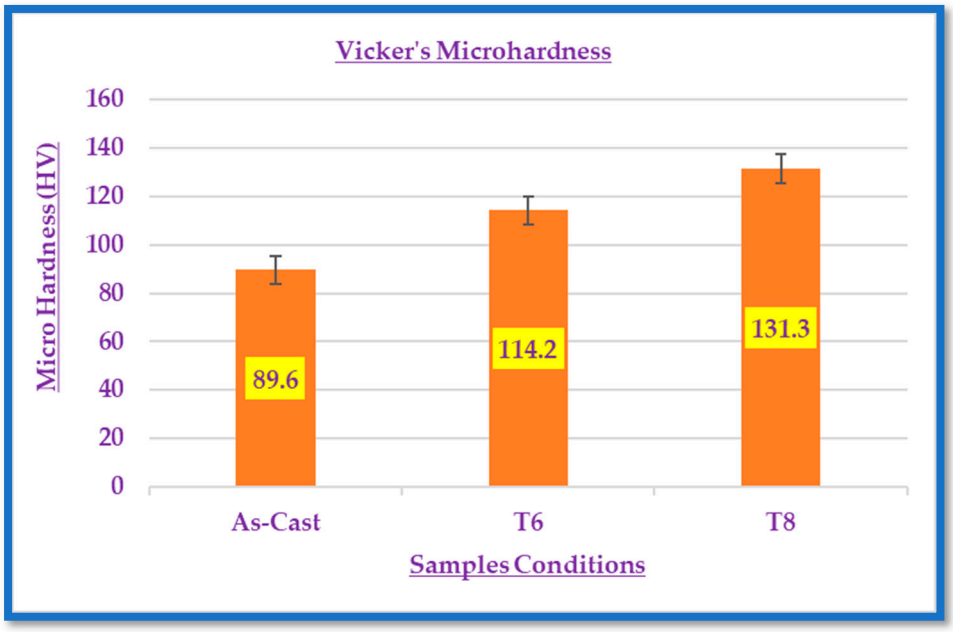

Figure 9. Vicker's microhardness analysis of AA2219/graphene matrix composites.

Table 2. Vickers hardness of AA2219/graphene composites under different conditions.

S. No:	Condition	Vickers Hardness (HV)
1.	As-Cast	89.6 ± 3.2
2.	T6	114.2 ± 2.7
3.	T8	131.3 ± 3.0

During heat treatment, the graphene surfaces serve as preferential nucleation sites for precipitate formation, leading to a more refined and homogeneously distributed precipitate structure for Al_2Cu and other strengthening phases. The thermal expansion mismatch between graphene and aluminium generates geometrically necessary dislocations around the reinforcement particles, creating additional strengthening through dislocation-based mechanisms, while the T8 condition's cold work prior to ageing further enhances precipitation kinetics and density, resulting in superior hardness values [30,31].

3.5. Ultimate Tensile Strength

Tensile tests were performed on both as-cast and heat-treated specimens using an INSTRON 8801 universal testing machine (Instron India Pvt. Ltd, Chennai, India) with a 100 kN load capacity. A constant crosshead speed of 0.5 mm/min was applied, and all tests were conducted in accordance with ASTM E8 standards. In this study, the AA2219–0.5 wt.% graphene composite exhibits a remarkable enhancement in tensile performance compared to the unreinforced alloy, with tunable strength–ductility characteristics achieved through tailored heat treatments. From Figure 10 and Table 3, in the as-cast state, the composite reaches an ultimate tensile strength (UTS) of 308.6 MPa ± 10.7 MPa at 13.68% elongation—an improvement attributable to the Hall–Petch grain refinement imparted by squeeze casting and Orowan strengthening from uniformly dispersed graphene nanoplatelets introduced via ball milling and ultrasonic stirring.

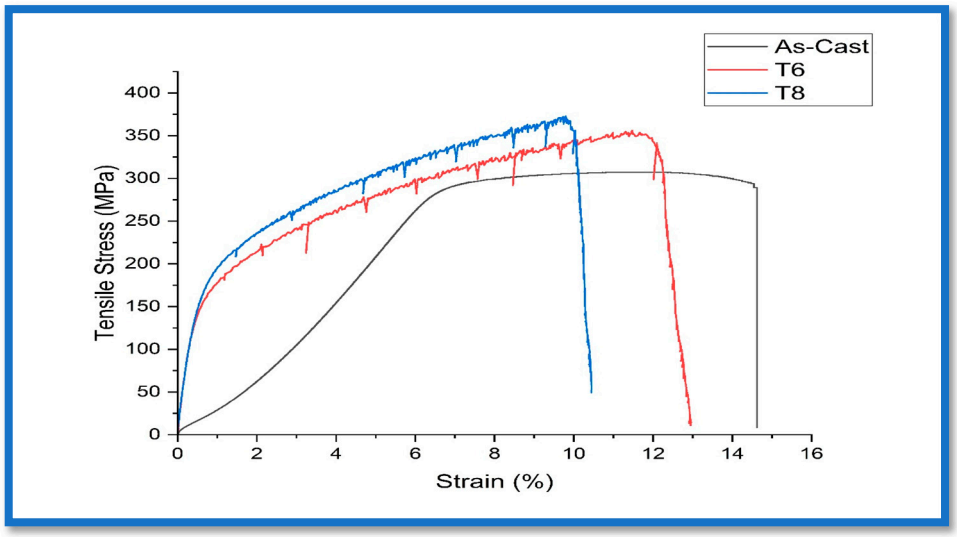

Figure 10. Ultimate strength analysis of AA2219/graphene matrix composites.

Table 3. Ultimate tensile strength and elongation of AA2219/graphene composites.

Condition	Ultimate Tensile Strength (MPa)	Elongation (%)
As-Cast	308.6 ± 6.5	13.68
T6	353.6 ± 5.1	11.24
T8	371.5 ± 4.8	8.54

A subsequent T6 ageing cycle further elevates the UTS to 353.6 MPa ± 8.5 MPa, driven by the precipitation of fine, semi-coherent θ′ (Al_2Cu) phases that act as potent obstacles to dislocation motion; however, elongation decreases moderately to 11.24% due to the dominance of precipitate hardening. The T8 treatment, which incorporates a cold-work step prior to ageing, maximises the UTS at 371.5 ± 9.6 MPa by promoting a more uniform θ′ distribution and heightened dislocation density, albeit at the expense of ductility (8.54% elongation). The Young's modulus of the graphene-reinforced AA2219 composites was evaluated under different processing conditions. For the as-cast composite, the modulus was measured at 62 GPa. The T6 heat-treated sample exhibited a higher modulus of 67 GPa. With T8 treatment, the modulus further increased to 71 GPa. This trend indicates a progressive enhancement in elastic stiffness with advanced processing. The increase is mainly attributed to microstructural refinement and improved graphene dispersion. These findings confirm the effectiveness of the employed processing routes in optimizing the composite's elastic properties.

During ageing, dynamic strain ageing and the associated PLC serrations—arising from solute (Cu/Mg) pinning and unpinning of dislocations—boost flow stress and work-hardening rates. Additionally, pre-strain in the T8 condition traps dislocations and internal stresses that foster uniform θ′ precipitation and back-stress hardening, while quenched residual stresses from the graphene–Al CTE mismatch further impede dislocation motion. Throughout deformation, dislocations accumulate at Al–graphene interfaces, reinforcing work-hardening through dislocation–graphene interactions and enabling efficient load transfer across robust Al–C interfaces [32,33]. By synergistically combining mechanical alloying, ultrasonic-assisted stir casting, squeeze casting, and optimized heat-treatment schedules, the composite delivers a controllable strength–ductility balance ideally suited for demanding aerospace applications.

3.6. Tensile Fractography Analysis

The fractography analysis of tensile fracture surfaces for graphene-reinforced AA2219 composites, as shown in Figure 11a–c, provides critical insight into the failure mechanisms under different processing conditions. The as-cast specimen (a) exhibits a predominantly brittle fracture surface characterized by irregular cleavage facets and limited evidence of plastic deformation, suggesting that crack propagation occurs rapidly through the microstructure. In contrast, the T6 heat-treated sample (b) reveals a more ductile morphology, with numerous deep dimples and extensive microvoid coalescence, indicating enhanced plasticity and energy absorption prior to fracture. The T8 condition (c) displays an even finer and more uniform distribution of dimples, reflecting a further improvement in ductility and toughness due to increased dislocation density and the refined precipitate structure induced by prior cold working.

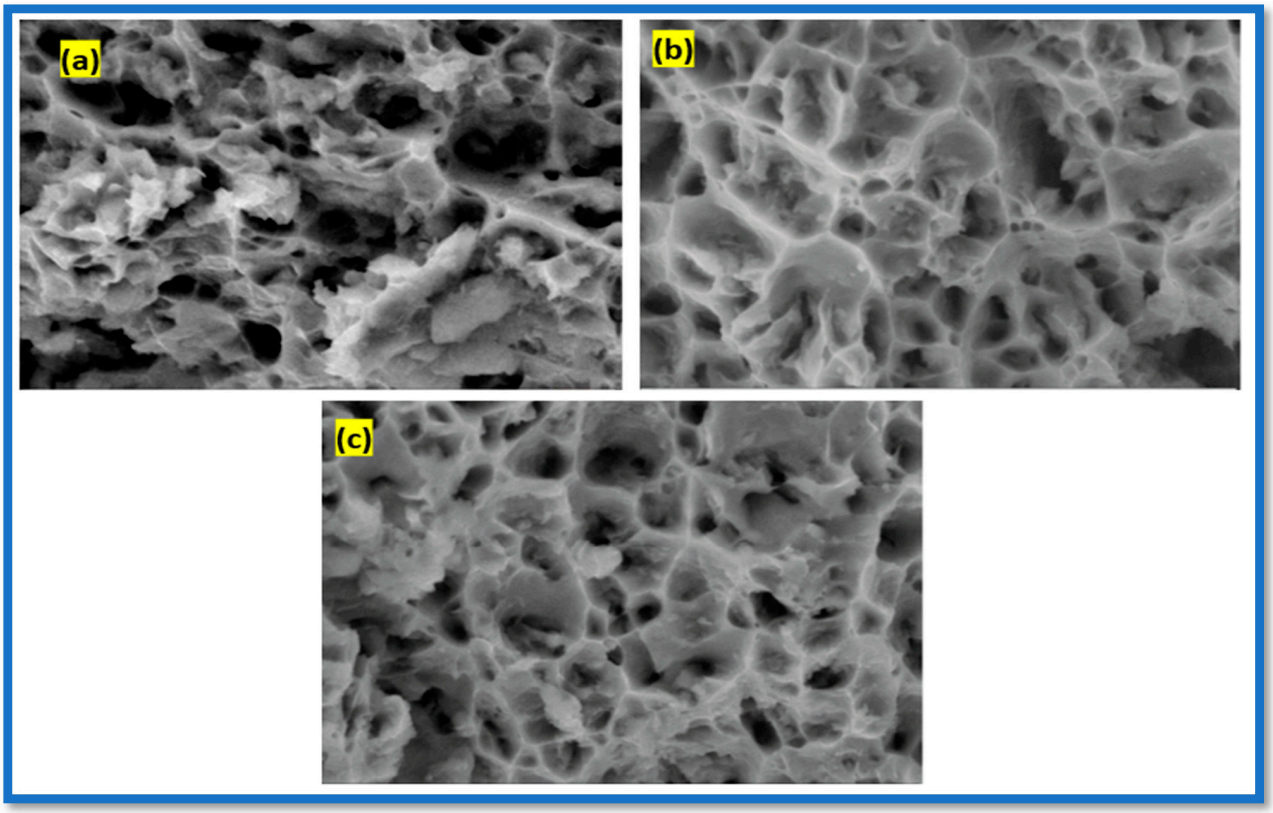

Figure 11. FE-SEM micrographs of the tensile fracture surface of AA2219/graphene composites: (**a**) as-cast, (**b**) T6, and (**c**) T8.

Quantitative fractographic analysis was performed on the SEM images of the fracture surfaces for the as-cast, T6, and T8 samples. The as-cast sample exhibited an average dimple diameter of approximately 0.9 μm, with a dimple density of 0.64 dimples per μm^2. Following T6 heat treatment, the average dimple size increased to 1.3 μm, while the dimple density decreased to 0.43 dimples per μm^2, reflecting enhanced ductility and a more homogeneous plastic deformation. In contrast, the T8 condition displayed a finer microstructure, with an average dimple diameter of 0.8 μm and a notably higher dimple density of 0.93 dimples per μm^2. This progression indicates that the combined effects of cold working and ageing in the T8 condition promote the formation of smaller and more densely distributed dimples, which are associated with improved microstructural refinement and increased resistance to crack propagation. These results clearly demonstrate the influence of processing and heat treatment on the fracture morphology and underlying mechanical behaviour of the graphene-reinforced AA2219 composites.

These microstructural transitions from brittle to ductile fracture modes are a direct consequence of heat treatment, with graphene reinforcement promoting crack deflection and bridging, thereby impeding crack growth [34,35]. Overall, the evolution in fracture features across the three conditions highlights the vital role of both graphene addition and tailored heat treatment in optimizing the strength–ductility synergy of AA2219 composites.

3.7. Surface Energy Measurement

The interfacial properties of the AA2219–graphene composites were systematically evaluated for the as-cast, T6, and T8 conditions. The contact angle of water on polished composite surfaces was measured for each condition using the sessile drop method with a contact angle goniometer, providing direct assessment of surface wettability. The obtained contact angles were 72° for as-cast, 68° for T6, and 65° for T8. These values were used to calculate the surface energy of the composite surface by applying the Owens–Wendt method, which separates the surface energy into polar and dispersive components based on the measured contact angle. The resulting surface energy values were 112 mJ/m^2 (as-cast), 128 mJ/m^2 (T6), and 145 mJ/m^2 (T8). To quantify the strength of interfacial bonding, the work of adhesion (W_{ad}) between the aluminium matrix and graphene was estimated theoretically using the geometric mean approach (a simplified Dupré Equation (1)) [32]:

$$W_{ad} = 2\sqrt{\gamma_{\mathbf{composite}} \cdot \gamma_{\mathbf{graphene}}} \quad (1)$$

where $\gamma_{\mathbf{composite}}$ is the measured surface energy for each condition and $\gamma_{\mathbf{graphene}}$ is 47 mJ/m^2. The calculated work of adhesion values were 145 mJ/m^2 (as-cast), 155 mJ/m^2 (T6), and 165 mJ/m^2 (T8). These improvements are a direct result of the processing methods employed—high-energy ball milling and ultrasonic-assisted stir casting—along with subsequent heat treatments, all of which promote better wettability, increased surface activation, and stronger interfacial bonding. In addition, the Lewis acid–base interactions at the interface were enhanced through exposure of fresh aluminium surfaces and graphene edges, with the amphoteric AA2219 acting as both acid and base and graphene functioning as a Lewis base. The synergistic increase in surface energy and the work of adhesion across all conditions, confirmed by both experimental measurement and theoretical calculation, underpins the improved mechanical properties, ductility, and stability observed in the composites.

4. Conclusions

This research presents the development of AA2219 matrix composites reinforced with 0.5 wt.% graphene nanoplatelets, utilizing an innovative combination of high-energy ball milling, ultrasonic-assisted stir casting, and squeeze casting techniques. The fabricated

composites were subjected to T6 and T8 heat treatments to optimize microstructure and mechanical performance. The study comprehensively evaluates the effects of graphene addition and heat treatment on the grain structure, hardness, tensile strength, and fracture behaviour of the composites. The specific inferences drawn from these investigations are summarized as follows:

- The combination of high-energy ball milling, ultrasonic stirring, and squeeze casting successfully ensured uniform dispersion of 0.5 wt.% graphene in the AA2219 matrix, while also reducing porosity and improving interfacial bonding.
- The T6 heat-treated samples exhibited a significant increase in hardness to 114.2 HV and an ultimate tensile strength of 353.6 MPa owing to the formation of fine and coherent θ' (Al_2Cu) precipitates that enhanced strength while maintaining moderate ductility at 11.24%.
- The T8 samples achieved the best mechanical performance, with a maximum hardness of 131.3 HV and ultimate tensile strength of 371.5 MPa. This improvement is attributed to the combined effects of cold working and ageing, which introduced dense dislocations and a refined precipitate structure.
- Heat treatment led to marked grain refinement, with average grain sizes reducing from ~75 μm in the as-cast condition to ~50 μm after T6 treatment and further down to ~21 μm in the T8 condition, contributing significantly to strength enhancement.
- Fractography showed a clear transition from brittle fracture in the as-cast condition to ductile features such as deep dimples and microvoid coalescence in T6 and T8 samples, confirming improved toughness and energy absorption during fracture.
- The lightweight nature, improved strength, and excellent thermal stability of the developed composite make it a promising material for hydrogen storage tanks in aerospace propulsion systems, supporting safe and efficient fuel containment.

Author Contributions: B.P.: writing—original draft preparation, formal analysis, and investigation. A.X.M.: methodology, materials, experimentation, and supervision, A.P.: supervision, validation, and manuscript editing. S.P.: validation and final manuscript. A.B.: validation and manuscript editing. All authors have read and agreed to the published version of the manuscript.

Funding: This research received no external funding.

Data Availability Statement: The data will be made available upon request.

Acknowledgments: The authors sincerely thank Vellore Institute of Technology, Vellore, for providing the necessary facilities for the fabrication, characterization, and testing of the composite materials.

Conflicts of Interest: The authors declare that they have no known competing conflicts of interest or financial interests.

References

1. Tenali, N.; Ganesan, G.; Babu, P.R. An investigation on the mechanical and tribological properties of an ultrasonic-assisted stir casting Al-Cu-Mg matrix-based composite reinforced with agro waste ash particles. *Appl. Eng. Lett.* **2024**, *9*, 46–63. [CrossRef]
2. Krstić, J.; Jovanović, J.; Gajević, S.; Miladinović, S.; Vaxevanidis, N.M.; Kiss, I.; Stojanović, B. Application of metal matrix nanocomposites in engineering. *Adv. Eng. Lett.* **2024**, *3*, 180–190. [CrossRef]
3. Veličković, S.; Miladinović, S.; Stojanović, B.; Nikolić, R.R.; Hadzima, B.; Arsić, D. Influence of load and reinforcement content on selected tribological properties of Al/SiC/Gr hybrid composites. *Prod. Eng. Arch.* **2018**, *18*, 18–23. [CrossRef]
4. Kareem, A.; Qudeiri, J.A.; Abdudeen, A.; Ahammed, T.; Ziout, A. A review on AA 6061 metal matrix composites produced by stir casting. *Materials* **2021**, *14*, 175. [CrossRef] [PubMed]
5. Karthik, A.; Karunanithi, R.; Srinivasan, S.A.; Prashanth, M. Microstructure and mechanical properties of AA 2219-TiB_2 composites by squeeze casting technique. *Mater. Today Proc.* **2020**, *27 Pt 3*, 2574–2581. [CrossRef]
6. Ajith, K.M.; Nirmal, U. AA2219 aluminum alloy reinforced with graphene: An overview. *Mater. Res. Express* **2020**, *7*, 086546.

7. Ashwath, P.; Venkatraman, M.; Patel, A.; Xavior, M.A.; Batako, A. Innovation in sustainable composite research: Investigating graphene-reinforced MMCs for liquid hydrogen storage tanks in aerospace and space exploration. *J. Mater. Res. Technol.* **2024**, *33*, 4313–4331. [CrossRef]
8. Alidokht, S.A.; Salehi, M.T.; Besharati Givi, M.K. Recent progress on graphene-based nanocomposites for aerospace applications. *Aerospace* **2021**, *8*, 20. [CrossRef]
9. Xavior, M.A.; Ranganathan, N.; Kumar, H.P.; Joel, J.; Ashwath, P. Mechanical properties evaluation of hot extruded AA 2024—Graphene nanocomposites. *Mater. Today Proc.* **2018**, *5*, 12519–12524. [CrossRef]
10. Liu, J.; Xu, C.; Liu, Y.; Li, F. Advances in the application of graphene-reinforced aluminum matrix composites. *Compos. Part A Appl. Sci. Manuf.* **2018**, *111*, 20–30. [CrossRef]
11. Pazhani, A.; Venkatraman, M.; Xavior, M.A.; Moganraj, A.; Batako, A.; Paulsamy, J.J.; Bavan, J.S. Synthesis and characterisation of graphene-reinforced AA 2014 MMC using squeeze casting method for lightweight aerospace structural applications. *Mater. Des.* **2023**, *230*, 111990. [CrossRef]
12. Sankaranarayanan, S.; Prabu, S.B.; Marimuthu, P. Mechanical properties of graphene-reinforced aluminum composites. *Metals* **2020**, *10*, 499. [CrossRef]
13. Hu, Z.; Zhao, Y.; Wang, J.; Wang, Z. Synthesis and strengthening mechanisms of graphene-aluminum composites. *Carbon* **2017**, *120*, 362–373. [CrossRef]
14. Prasad, S.V.; Asthana, R. Aluminum metal-matrix composites for automotive applications: An overview. *JOM* **2004**, *56*, 35–39.
15. Zuo, L.; Yu, S.; Wang, B.; Zhang, Z.; Liu, Y. Ultrasonic-assisted fabrication of aluminum-based composites: A review. *Ultrason. Sonochem.* **2019**, *52*, 206–219. [CrossRef]
16. Hashim, J.; Looney, L.; Hashmi, M.S.J. Metal matrix composites: Production by the stir casting method. *J. Mater. Process. Technol.* **1999**, *92–93*, 1–7. [CrossRef]
17. Mula, S.; Padhi, P.; Panigrahi, S.C.; Mohapatra, N. Effect of SiC content on the properties of aluminum matrix composite. *Mater. Sci. Eng. A* **2009**, *498*, 99–106. [CrossRef]
18. Choi, H.S.; Hwang, Y.J.; Lee, J.S. Recent advances in the preparation of graphene/aluminum composites by powder metallurgy routes. *Metals* **2021**, *11*, 817. [CrossRef]
19. Ma, Z.Y.; Wang, G.; Lei, T. The effect of ball milling on dispersion and properties of graphene reinforced Al composites. *J. Alloys Compd.* **2021**, *862*, 158171.
20. Li, Y.; Dong, H.; Wang, S. Squeeze casting of aluminum alloys and composites. *Metals* **2020**, *10*, 249. [CrossRef]
21. Chen, B.; Kondoh, K.; Imai, H.; Umeda, J. Fabrication of graphene/aluminum composites by powder metallurgy and hot extrusion. *J. Mater. Sci. Technol.* **2015**, *31*, 820–826.
22. Kumar, S.; Anand, A.; Pandey, K.M. Ultrasonic cavitation for the preparation of graphene and its composites. *Ultrason. Sonochem.* **2019**, *56*, 83–97. [CrossRef]
23. Bharathiraja, P.; Anthony Xavior, M. Effect of B4C and graphene on the microstructural and mechanical properties of Al6061 matrix composites. *J. Mater. Res. Technol.* **2024**, *31*, 496–505. [CrossRef]
24. Han, B.; Huang, X.; Huang, Q.; Zhang, L. Homogeneous dispersion of graphene in aluminum matrix using ball-milling. *Materials* **2022**, *15*, 48. [CrossRef]
25. Shao, X.; Wang, T.; Liu, Z. Effect of process parameters on the microstructure and mechanical properties of graphene reinforced Al composites. *J. Manuf. Process.* **2021**, *65*, 256–263. [CrossRef]
26. Wang, J.; Nie, J.; Zhu, X. Microstructural evolution and mechanical properties of AA2219 aluminum alloys. *Mater. Sci. Eng. A* **2017**, *698*, 371–380. [CrossRef]
27. Chai, G.; Chen, B.; Huang, Z. Precipitation hardening of AA2219 and its composites. *Metals* **2021**, *11*, 480. [CrossRef]
28. Sun, Y.; Wang, Z.; Wei, Y. Mechanical behavior and fracture characteristics of graphene/aluminum composites. *Materials* **2020**, *13*, 4765. [CrossRef]
29. Zhang, X.; Li, M.; Yang, H.; Yu, S. Effect of heat treatment on microstructure and mechanical properties of AA2219/SiC composites. *Mater. Sci. Forum* **2017**, *877*, 117–122.
30. Huang, Z.; Liu, X.; Xie, H.; Li, X. Fracture and strengthening mechanisms in graphene-reinforced aluminum composites. *Acta Mater.* **2019**, *166*, 507–519. [CrossRef]
31. Du, J.; Wang, X.; Zhai, W.; Liu, L. Effect of graphene content on the microstructure and mechanical properties of Al matrix composites. *Mater. Des.* **2018**, *142*, 174–184. [CrossRef]
32. Liu, Y.; Li, M.; Lu, Y. Grain refinement and mechanical properties of graphene reinforced Al composites. *Mater. Lett.* **2020**, *262*, 127044. [CrossRef]
33. Wu, B.; Chen, B.; Kondoh, K.; Wang, M. Fracture toughness improvement in graphene/Al composites. *Crystals* **2018**, *8*, 431. [CrossRef]

34. Esawi, A.M.K.; Farag, M.M. Carbon nanotube reinforced composites: Processing and mechanical properties. *Compos. Part A Appl. Sci. Manuf.* **2007**, *38*, 646–653. [CrossRef]
35. Rahimian, M.; Ehsani, N.; Parvin, N.; Baharvandi, H.R. The effect of particle size, sintering temperature, and sintering time on the properties of Al–Al_2O_3 composites, made by powder metallurgy. *J. Mater. Process. Technol.* **2009**, *209*, 5387–5393. [CrossRef]